Patient Specific Biomechanical Modeling of Hepatic Vasculature for Augmented Reality Surgery

Binh Phu Nguyen[1], Tao Yang[2], Florence Leong[2], Stephen Chang[3], S.H. Ong[1], Chee-Kong Chui[2]

[1] Department of Electrical and Computer Engineering, National University of Singapore, Singapore
{phubinh, eleongsh}@nus.edu.sg
[2] Department of Mechanical Engineering, National University of Singapore, Singapore
{yang.tao, florence.leong, mpecck}@nus.edu.sg
[3] Department of Surgery, National University Hospital, Singapore
surv7@nus.edu.sg

Abstract. This paper describes the generation of a patient specific biomechanical model of hepatic vasculature from clinical CT images. Three dimensional region growing, thinning and skeletonization are used to obtain an accurate vascular model. Control points are employed to represent the geometrical characteristics of the vascular skeleton. The topological and geometrical information of the vasculature tree is represented using generalized cylinders. A nonlinear constitutive equation is used to represent the material properties of the vessels. The vascular material properties are also dependent on the patient's age. The resultant biomechanical model is represented using VRML 2. We demonstrated the application of this model with a finite element simulation of a deformation due to the presence of a tumor.

Keywords: Modeling, segmentation, constitutive equations, liver.

1 Introduction

In augmented reality (AR) surgery, the surgeon is able to view the surgical plan that is overlaid on the surgical site using state-of-the-art interactive media and visualization technologies. However, the overlaid images are static models [1]. For example, the hepatic vasculature on the overlay plan will not deform when the liver is operated upon by the surgeon during surgery. A geometrical vasculature model or volume rendered image of the vasculature is incapable of realistic deformation. A patient specific biomechanical or physics based model is thus required [2], but there are many challenges in the creation of an accurate biomechanical model for AR surgery.

The biomechanical model should accurately represent the geometrical and topological information of the patient's hepatic vasculature. It should be a finite element (FE) model with appropriate nonlinear constitutive equations. For the model to be useful, the FE-based biomechanical model has to be computationally efficient so

that the surgeon is able to interact with it in real time during AR surgery. This paper describes the generation of a FE-based patient specific biomechanical model for AR surgery. A nonlinear constitutive law is proposed to represent the complex stress-strain relationship of hepatic vessel walls.

In Section 2, we describe the algorithm for obtaining the hepatic vasculature. This includes the steps of 3D region growing, thinning and skeletonization. We introduce a method of representing the skeleton using control points. In Section 3, we present a new material assignment scheme that is based on the patient's age and uses a new constitutive model. In Section 4, we describe the representation of the resultant biomechanical model using VRML 2. We also present a finite element (FE) simulation of the vascular model when subjected to compression by a nearby tumor. The paper is concluded in Section 5.

2 Materials and Methods

We hypothesize that a hepatic vessel can be represented by one or more FE beam elements. Such an element has a circular cross section and can be visualized as a generalized cylinder. This is a valid assumption of the hepatic vessels since they are typically small vessels. When filled with blood, they generally have a circular cross section.

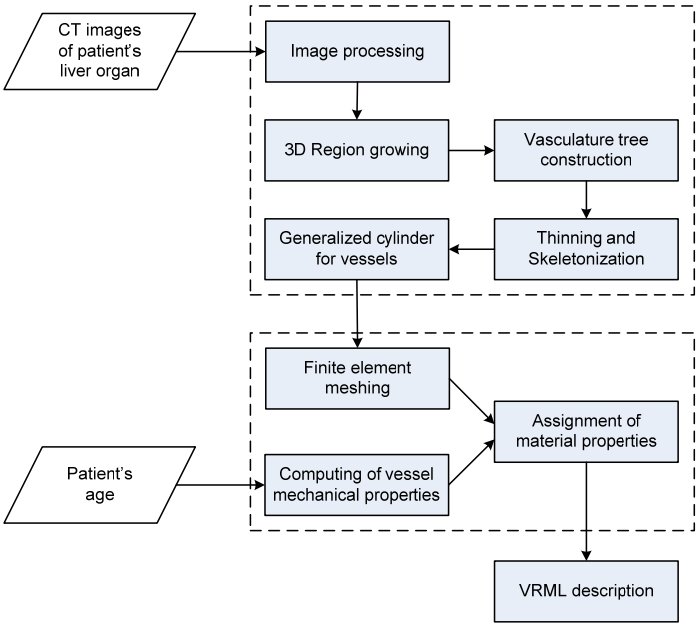

Fig. 1. Overview of the patient specific modeling processes.

A modified 3-D seeded region growing algorithm based on [5] is first applied to extract the raw regions of interest from CT images. A recursive search procedure is

implemented to dynamically establish the tree-like branching structure. Next, all tiny trees which do not meet predefined criteria will be removed from the structure. Finally, a thinning algorithm [6] is used to extract the skeleton of each region in the tree. The skeleton information and the branching structure will be used in modeling the hepatic vasculature. Details of the method are presented below.

2.1 3-D Region Growing

Let v denote the 3-D image, (x, y, z) denote a voxel in the image and $v(x, y, z)$ denote the intensity of voxel (x, y, z). The kth slide of v refers to all voxels having coordinate $z = k$. Before processing, the user predefines the intensity range for valid seeds and the allowed intensity for voxels in the final regions. The 3-D region growing algorithm involves two main steps: 2-D region growing on the individual slices and region merging between consecutive slices to form the complete 3-D regions.

1) 2-D seeded region growing on slice k

(a) Find the first unvisited voxel (x, y, k) which is in the allowed intensity range. Assign the next available region number to this voxel.

(b) Examine all unvisited neighbors of (x, y, k). Include the neighbor (x', y', k) recursively in this region if and only if it is a valid seed, or (x', y', k) is in the allowed intensity range and the intensity difference between it and (x, y, k) is small enough.

(c) Return to step (a) if more voxels on slice k still need to be examined.

(d) Generate the following information for each region on this slide: number of seeds, number of voxels, and dimensions of the bounding box.

2) Region merging for slide k and (k-1)

(a) Use bounding boxes of regions to locate all overlapping portions of the regions between the current (kth) slide and the previous ($(k-1)$th) slide.

(b) Merge two overlapping regions on the condition that, within the overlapping portion, the voxel (x, y, k) on the current slide has at least one neighbor $(x', y', k-1)$ which is a valid seed or its intensity is sufficiently close to $v(x, y, k)$.

(c) Update the dynamic double-linked list information for both regions which indicates that these regions can be merged.

2.2 Establishment of Tree Structure

Based on the double-linked list information of each region, a tree-like branching structure is dynamically established by a recursive traverse procedure through all linked regions. All possible vessel trees are created and a tree identification tag is attached to each corresponding region. After that, all trees with the total number of voxels and/or the total number of seeds less than the pre-specified numbers will be removed from the structure. It means that all regions belong to these trees will not be used in further steps. These regions can be removed based on their tree identification tags.

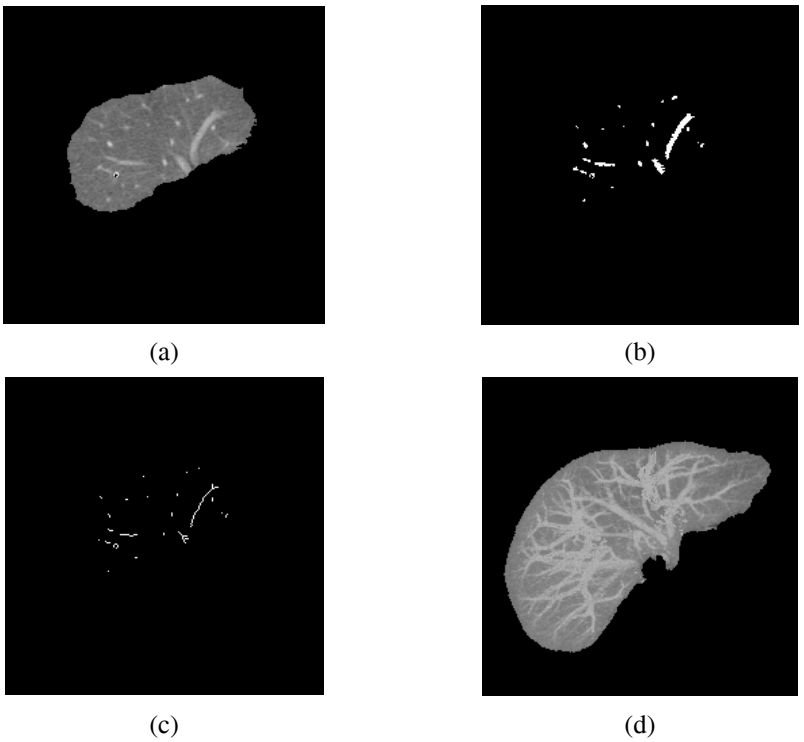

Fig. 2. (a) A 2-D slice cut from a 3-D CT scan of liver. The vessels appear as bright areas. (b) The regions on that slide. (c) The region skeletons after thinning step. (d) The maximum-intensity projection images for all slides.

2.3 Skeletonization Using Control Points

In the tree structure obtained in the previous step, a thinning procedure [6] is applied to all the remaining regions to extract their skeletons. This algorithm is

efficient and guarantees that the skeleton will be close to the center line of the region. In order to reduce the computational load and for ease of representing the skeleton in the form of a vessel, a finite number of control points is assigned to the skeleton, and subsequently the new skeleton is obtained by using straight lines to connect the control points.

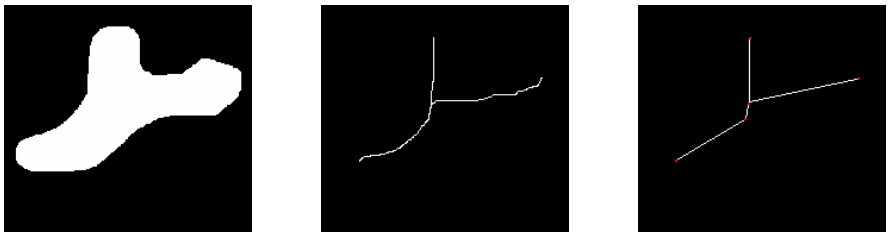

(a) (b) (c)

Fig. 3. (a) One 2-D region. (b) The region after thinning process. (c) Region skeleton representation by the lines connecting control points.

The Harris corner detector [8] is applied to extract the control points from the skeleton of a region. This method is used widely because of its strong invariance to rotation, scale, illumination variation and image noise. The detector is based on the local auto-correlation function of a signal, where the local auto-correlation function measures the local changes of the signal with patches shifted by a small amount in different directions.

Given a point (x, y) and a shift $(\Delta x, \Delta y)$, an approximate form of the auto-correlation function for a shifted image can be derived from Taylor's expansion truncated to the first order terms [9]. This is shown as follows:

$$f(x,y) = \sum_{W} \left(I(x_i, y_i) - \left(I(x_i, y_i) + \left[I_x(x_i, y_i) \quad I_y(x_i, y_i) \right] \begin{bmatrix} \Delta x \\ \Delta y \end{bmatrix} \right) \right)^2$$

$$= \begin{bmatrix} \Delta x & \Delta y \end{bmatrix} \mathrm{F}(x,y) \begin{bmatrix} \Delta x \\ \Delta y \end{bmatrix} \qquad (1)$$

where

$$\mathrm{F}(x,y) = \begin{bmatrix} \sum_{W} \left(I_x(x_i, y_i) \right)^2 & \sum_{W} I_x(x_i, y_i) I_y(x_i, y_i) \\ \sum_{W} I_x(x_i, y_i) I_y(x_i, y_i) & \sum_{W} \left(I_y(x_i, y_i) \right)^2 \end{bmatrix}$$

In the above equations, I denote the image function and (x_i, y_i) are the points in the windows W centered on the point (x, y). I_x and I_y denote the partial derivative in x and y, respectively. Matrix F captures the intensity structure of

the local neighborhood. Let λ_1, λ_2 be the eigenvalues of F. The eigenvalues form a rotationally invariant description. Appropriate actions will be taken for the three cases: (1) both λ_1, λ_2 are small, (2) one eigenvalue is high and the other is low, and (3) both eigenvalues are high. Only case (3) implies the applicability of a control point.

After the set of control points in each region is obtained, the skeleton of the 3D vessel tree structure is represented by the set of lines connecting the control points in the parent-children relationship regions. These lines will be the central lines of the cylinders representing the vessel. The use of control points in the skeletonization process is computationally faster compared to conventional methods and hence more suitable for AR applications.

3 Constitutive Law of Hepatic Vessel Walls

The combined logarithmic and polynomial based strain energy function [3] is used to model the stress-strain relationship of the vessel walls. The combined strain energy function is given by

$$W = \frac{-C_1}{2} In(1-u) + \frac{q}{2} \tag{2}$$

where

$$u = \frac{1}{2}C_2(I_1-3)^2 + \frac{1}{2}C_3(I_4-1)^2 + C_4(I_1-3)(I_4-1)$$
$$q = C_5(I_1-3)^2 + C_6(I_4-1)^2 + 2C_7(I_1-3)(I_4-1)$$

$W, I_1, I_4, C_{1,\ldots,7}$ are the strain energy, first invariant, fourth invariant and material constants, respectively.

We assume that the hepatic vascular system comprises mainly elastic arteries and veins, with characteristics close to that of the abdominal aorta. Fig. 4 compares the experimental and theoretical stress-strain relationship of the vessel walls in the longitudinal direction. Experimental data are based on [4], which were acquired from subjects between 20 and 29 years of age.

A multiplier k is introduced to accord for the variation of stress-strain properties due to aging. Typically, the tensile strength of blood vessels decreases as one ages. For a person aged between 20 and 29 years, $k = 1$, while $k = 0.75$ for ages between 30 and 39 years. We have

$$\mathbf{S} = k \times \frac{\partial W}{\partial \mathbf{E}} \tag{3}$$

where $\mathbf{S}$ is the Piola-Kirchoff stress tensor and $\mathbf{E}$ is the Green-Lagranger strain tensor.

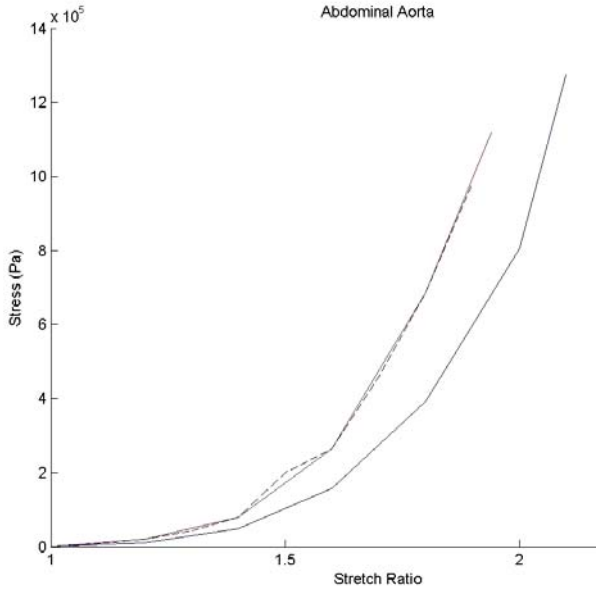

Fig. 4. Experimental and theoretical stress-strain relationships. In the experiment [4], there are 28 subjects between 20 and 29 years of age. Red solid line: experimental data along longitudinal direction; blue solid line: experimental data along transverse direction; black dotted line: theoretical estimation.

In this paper, we use the VRML 2 format to construct the vascular tree with some additional tags to represent the mechanical properties of a vessel. The tags carry information such as strain and strain energy and are obtained from experimental data.

4 Results

Fig. 5 is a snapshot of the resultant hepatic vasculature tree represented using VRML 2. The deformation of a segment of the vasculature tree can be analyzed by the finite element method. A commercial FE software (Ansys Multiphysics) is employed for finite element simulation. As shown in Fig. 6, the meshed model is a finite element model of a Y-shaped hepatic vessel. The main vessel has a diameter of 8 mm and the branch vessel has a diameter of 7 mm. We assume that a wall thickness is 1 mm, and the vascular height is 40 mm. The vessel is considered an isotropic elastic material as described in Section 3. We also assume that the Poisson ratio is 0.4. A tumor (not shown in Fig. 6) is lying on the main vessel. We assume that a pressure of 3,900Pa is imposed on the area. This is equivalent to a compressive force of 5N, which resembles the force experiment during a delicate manipulation of the tumor.

The three outlets seen in Fig. 6 are constrained from all freedom. The solid model in Fig. 6(a) shows the deformation of the vessel under a static uniform pressure load resulting in a maximum displacement of 2.63 mm. Fig. 6(b) shows the stress distribution from the instantaneous deformation. The maximum stress, 66,307Pa, appears at the contacting region between tumor and vessel, and is transmitted to the branch vessel as shown in the figure.

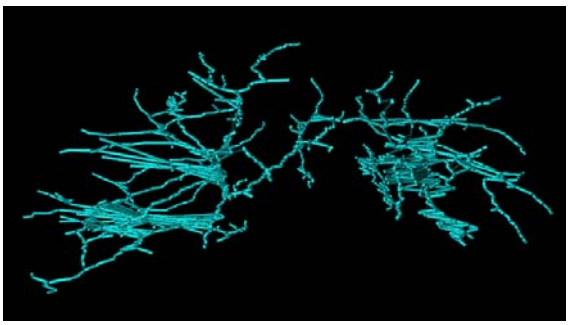

Fig. 5. The resultant biomechanical model is represented using VRML 2

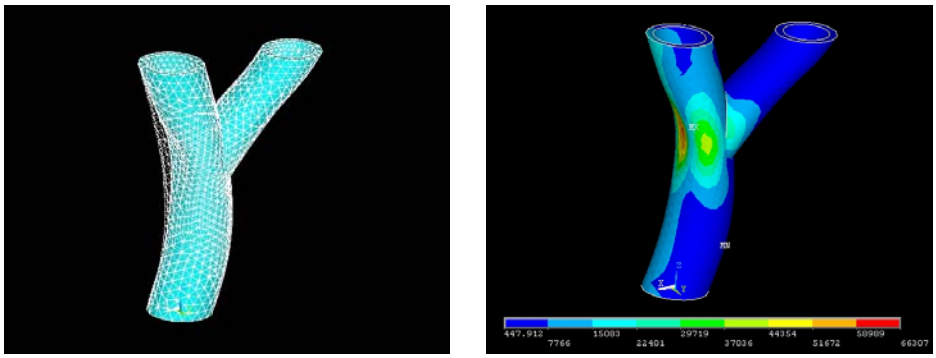

(a) (b)

Fig. 6. (a) Deformation of vessel, the entirety in light blue color is the deformed vessel, and the mesh on the left hand side shows the unreformed entirety. (b) Stress distribution in vessel, red spot, the area of contact in the graft, shows the highest stress. The tumor which is not shown, compressed on the vessel and caused the vessel to deformed, the stress is transmitted to the branch vessel as show on the right side vessel.

5 Discussion and Concluding Remarks

The reconstructed model of hepatic vasculature is represented as a skeleton. A skeleton is a graph whose vertices corresponding to joints and whose edges correspond to line segments between two joints that share a parent-child relationship. In other words, the line segment represents a segment of hepatic vessel, and the joint

is a place where hepatic vascular branches. Our approach is different from the skeleton complex defined in [7] in that the deformation of the skeleton is nonlinear, and each line segment is to be modeled as a finite beam element. The vascular wall is assumed to be rigid. In order to be compatible with existing computer graphics rendering, we adopted the VRML format with additional tags to include mechanical properties components. A customized FE solver is required for the simulation.

The variation of diameters along a vessel needs further image processing and the segmentation algorithm can be improved. The diameter of each vessel can be derived from the corresponding information of each region, such as the number of seeds and voxels. It is important to keep track of the vascular diameters, because the size of vessel plays an important part in stress and deformation analyze.

Vascular tissue is not isotropic material, however. The constitutive equation introduced in this paper and the assumptions made in the simulation provide us a better understanding of the vessel response to external force. It also gives quantitative information about deformation and stress distribution, which is very useful in surgery planning. In future work, the vasculature will be considered a transverse isotropic material, and another constitutive equation will be introduced to represent the vasculature properties.

Acknowledgements. This research is supported by a research grant from National University of Singapore (R-265-000-270-112 and R-265-000-270-133).

References

1. Fischer, G. S., Deguet, A., Schlattman, D., Taylor, R., Fayad, L., Zinreich, S. J., and Fichtinger, G.: MRI Image Overlay: Applications to Arthrography Needle Insertion. Studies in Health Technology and Informatics 119, 150-155 (2005).
2. Teo, J. C., Chui, C. K., Wang, Z. L., Ong, S. H., Yan, C. H., Wang, S. C., Wong, H. K., and Teoh, S. H.: Heterogeneous meshing and biomechanical modeling of human spine. Medical Engineering and Physics 29(2), 277-290 (2007).
3. Chui, C., Kobayashi, E., Chen, X., Hisada, T., and Sakuma, I.: Combined compression and elongation experiments and non-linear modeling of liver tissue for surgical simulation. Medical and Biological Engineering and Computing 42(6), 787-798 (2004).
4. Yamada, H.: Strength of Biological Materials. The Williams & Wilkins Company, Baltimore, Maryland (1970).
5. Wan, S. Y., Kiraly, A. P., Ritman, E. L., and Higgins, W. E.: Extraction of the Hepatic Vasculature in Rats using 3-D Micro-CT images. IEEE Transactions on Medical Imaging 19(9), 964-971 (2000).
6. Joseph, M. C.: Efficient binary image thinning using neighborhood maps. In: Paul, S. H. (eds.) Graphics Gems IV. Academic Press (1994).
7. Steve, C., Seth, G., Brian, C., Tom, D., and Zoran, P.: Interactive skeleton-driven dynamic deformations. ACM Transactions on Graphics 21(3), 586-593 (2002).
8. Chris, H. and Mike, S.: A combined corner and edge detector. In: Proceedings of 4th Alvey Vision Conference, pp 147-151. Manchester (1988).
9. Lee, N. Y., Kim, G. Y and Choi, H. I.: 3D Modeling of the Vessels from X-Ray Angiography. In: Digital Human Modeling. LNCS, vol. 4561, pp. 646-654. Springer Berlin, Heidelberg (2007).